Visentin, Sonja; Barbero, Nadia; Bertani, Francesca Romana; Guidi, Mariangela Cestelli; Ermondi, Giuseppe; Viscardi, Guido; Mussi, Valentina. Multivariate analysis applied to Raman mapping of dye-functionalized carbon nanotubes: A novel approach to support the rational design of functional nanostructures. ANALYST. 140 (16) pp: 5754-5763.
DOI: 10.1039/c5an00820d

Multivariate Analysis Applied to Raman Mapping of Dye-Functionalized Carbon Nanotubes: a Novel Approach to Support the Rational Design of Functional Nanostructures

Sonja Visentin[a], *Nadia Barbero*[b], *Francesca Romana Bertani*[c], *Mariangela Cestelli Guidi*[d], *Giuseppe Ermondi*[a], *Guido Viscardi*[b] *and Valentina Mussi*[c,*]

[a] *Department of Molecular Biotechnology and Health Science, University of Torino, Via Nizza 52, Torino, 10126, Italy*

[b] *Department of Chemistry, Interdepartemental Centre NIS, University of Torino, Via P. Giuria 7, 10125 Torino, Italy*

[c] *Institute for Complex Systems, National Research Council (ISC-CNR), Via del Fosso del Cavaliere 100, Rome, 00133, Italy*

[d] *Laboratori Nazionali di Frascati INFN, Via E. Fermi 40, Frascati, 00044, Italy*

Abstract

Principal Component Analysis is applied to analyse the Raman maps collected on carbon nanotubes at different degree of oxidation and functionalization with dye labeling molecules. The results are used to demonstrate that the technique is extremely effective in clustering the data and comparing preparation protocols, so that it allows to draw a fast and reliable classification of the molecule propensity to interact with pristine and oxidized carbon nanotubes. The spectral findings are supported and elucidated by several experimental techniques, thermogravimetry and steady-state and time-resolved fluorescence measurements, and by computational modeling, showing that the proposed methodology could represent a powerful and routine test for the rational design of functional nanostructures.

1. Introduction

It is nowadays clear that present developments in the field of nanostructured materials and nanotechnology will have a profound impact in several areas, from energy technologies to biotechnological and medical applications. The current efforts and findings will probably lead to a drastic change of methodologies, analytical instruments and diagnostic tools, and will modify the way we approach the problems of environmental and clinical monitoring, energy storage and tissue

* Corresponding author. Tel. +390649934166. E-Mail: valentina.mussi@isc.cnr.it (Valentina Mussi)

engineering, biomarking and drug delivery. The dimensional reduction to the nanoscale is in fact associated to a substantial modification of the material's optical, electronic and structural properties, so that the creation of novel functional materials with unique features becomes possible. At the same time, nanomaterials offer the opportunity to probe and influence processes and samples at the cellular and molecular level, enabling the possibility for early diagnosis, improved prognosis, targeted therapeutic action and imaging with higher specificity and resolution.

However, especially when dealing with applications in the biomedical field, the use of nanostructured materials forces us to face problems related to the development of reliable tools for a detailed characterization of their properties and for an accurate proof of their actual effectiveness. We need to know what we use, follow and demonstrate the operation, monitor the interaction with the environment and with biological samples and other materials, so to have appropriate instruments to optimize the design and synthesis of new nanoscale structures. This is even more true when dealing with nano-biocomposites and hybrid materials, such as functionalized carbon nanotubes (CNT), for purposes of targeting, detection, implant construction, delivery and imaging [1]. Indeed, CNTs possess special mechanical, optical and electrical properties, that can be further tuned via coupling and surface modification to attain novel functionalities. As an example, such carbon based tubular structures have been very recently used to incorporate and protect aggregated dye molecules in order to obtain a giant Raman scattering usable for multispectral imaging [2]. As proposed by the authors, this notable effect, being free from fluorescence background and photobleaching, can be exploited to build a library of *functionalized* nanoprobe labels for Raman imaging. However, CNTs themselves are very strong Raman scatterers with peculiar spectral features that are subtly modified depending on the specific method applied for their functionalization, via specific or unspecific bonding, and on the type, distribution, and concentration of compounds or inorganic nanoparticles attached on their surface.

Here we propose to apply Multivariate Analysis to Raman mapping of single wall carbon nanotubes treated with different fluorescent dyes and different coupling approaches as a valuable tool to verify

the efficiency of the functionalization procedure, to compare the effects of various labels, to study the homogeneity of the final sample and to perform dosing and toxicology studies for bio-imaging and delivery applications. Actually, the fact that a specific dye/drug linked to CNTs for biomedical or imaging applications gives a non–homogeneous sample does not make it a good candidate, because, as a consequence, the ultimate dose of the dye/drug is not controllable. Moreover, very often it is not sufficiently taken into account that the nanomaterial acting as a carrier should be considered as a drug itself to all effects, and therefore has to be accurately characterized in order to obtain reproducible dose-effect data and trustworthy toxicological tests, such as those just based on Raman measurements proposed in [3]. Obviously, the simple information obtainable with standard techniques shows that the molecule is effectively able to bind to the nanostructure, but it does not tell us anything about quantitative aspects of the interaction. In this context, we demonstrate that Principal Component Analysis (PCA) applied to Raman mapping constitutes a very robust method, allowing a rapid and reliable classification of CNT-based samples, which is fundamental to improve the design of the nanostructure and to optimize the preparation procedure for the specific application. A similar approach has been applied in [4] to discriminate the Raman spectra of functionalized multiwalled carbon nanotubes with respect to pristine ones, but presented data are poorly clustered and separated, and there is no comparison between different functionalization molecules and protocols. Here, the results of Multivariate Analysis on both specific and non specific modifications obtained with three dyes, rhodamine 6G (R6G), cyanine 3 (Cy3) and thionin acetate (THA), at different aging status, are supported and elucidated by steady-state and time-resolved fluorescence measurements, thermo-gravimeter analysis (TGA) and Computational Modeling, showing that the methodology can rightly aspire to become an alternative powerful and routine test for CNT-based functional nanostructures.

2. Experimental

2.1 Functionalization

An ethanolic solution of the three dyes (4.3 x 10^{-6}M THA, 1.67 x 10^{-5}M R6G, 1.0 x 10^{-6}M Cy3) was added to a small amount (2 mg) of single walled CNTs; the solid was tread on, and the mixture is allowed to stand at room temperature for 30 min. After centrifugation (10000 rpm for 10 min) CNTs have been removed and the solution filtered on a 0.45 μm pore filter. Fluorescence spectra (scan speed 100 nm/min) were recorded in the range of 600–700 nm upon excitation at 594 nm. Excitation and emission slits were 10.0 nm and 5.0 nm, respectively.

A daily fresh three to five points (from 9.7 x 10^{-8} to 2.4 x 10^{-7}; stock solution 9.7 x 10^{-5}) calibration graph of the dyes was done using the fluorimetric method herein described (R^2 = 0.999, see SI).

2.2 Raman spectroscopy and mapping

Raman maps are recorded with a dispersive Raman Microscope (XploRA, HORIBA Jobin Yvon S.A.S., France). The measuring conditions are: 532 nm excitation wavelength, 500 μm wide confocal hole, 200 μm wide entrance slit, 100x objective lens, 1200 gr/mm grating. The powder/flake samples are directly deposited on a glass slide and the maps are realized by collecting 49 spectra point-by-point on an area of 6x6 μm^2 with a step size of 1 μm. The measured spectral range is 74-2700 cm^{-1}, and each spectrum results from 10 accumulations acquired with the Autofocus function turned on (range from -3 μm to 3 μm with a step size of 0.5 μm).

Single Raman spectra have been acquired at fixed positions by using the same measuring conditions of the maps.

2.3 Principal Component Analysis

PCA is performed valuating the Raman intensities over 114 discrete wavelengths, chosen in the spectral ranges corresponding to the RBM, D, G, M and G' bands (the used wavelengths are detailed in Table S1 of the SI). The analysis is executed computing the correlation matrix instead of the covariance one, because, even if the data are uniform in terms of type, they are not homogeneous in terms of the range of variability: the measured Raman intensities in the case of the spectra obtained on pristine carbon nanotubes are up to 100 times higher than that collected in the

case of the oxidized and functionalized samples. Actually, the positioning of the points in the final score plot is only partially affected by this choice, but clusters are less compressed and more readable if analyzed by means of the correlation matrix, as can be verified by looking at the comparison shown in Figure S3 of the SI.

2.4 Computational methods

The 3D structures of investigated compounds, thionine acetate (THA), cyanine and rhodamine, are prepared using the building tool provided by Spartan '10 molecular modeling software [5]. The starting geometries are fully optimized without symmetry constraints using the semiempirical quantum-mechanical AM1 Hamiltonian [6] as implemented in Spartan '10. Then, minimized structures are submitted to GRID/BIOCUBE4mf procedure [7]. The program BIOCUBE4mf filters MIF points calculated with GRID [8] according to user-specified threshold values (-1.0 both for DRY and Car, -3.0 kcal/mol for O-).

2.5 Thermogravimetric Analysis (TGA)

TGA experiments were performed on approximately 10 mg of the samples with a 60 cm^3/min nitrogen flow (99,999 % purity) and with a 10°C/min heating ramp using a TGA Q600 SDT instrument.

2.6 Photoluminescence Spectroscopy

Photoemission steady-state spectra were acquired with a Horiba Jobin Yvon Fluorolog3 TCSPC spectrofluorimeter equipped with a 450 W Xenon lamp and a Hamamatsu R928 photomultiplier. The spectral response was corrected for the spectral sensitivity of the photomultiplier.

Fluorescence lifetimes, τF, were measured using a time-correlated single photon counting (TCSPC) technique (Horiba Jobin Yvon) with excitation source NanoLed at 455 nm (Horiba) and impulse repetition rate of 1 MHz to a TBX-4 detector. The detector was set to 550 nm for rhodamine 6G, 615 nm for THA and 560 nm for cyanine with a 14 nm band pass. The instrument was set in the Reverse TAC mode, where the first detected photon represented the start signal by the time-to-

amplitude converter (TAC), and the excitation pulse triggered the stop signal. DAS6 decay analysis software was used for lifetime calculation.

3. Results

3.1 Raman analysis

3.1.1 Raman spectra

Figure 1 presents single Raman spectra collected on the pristine carbon nanotube powder sample (black solid line), on the single walled CNT (SWCNT) sample subjected to chemical oxidation, o-SWCNTs (magenta dash-dotted line), and on the SWCNT sample treated with Cy3 dye before (grey dotted line) and after (green dashed line) the oxidation.

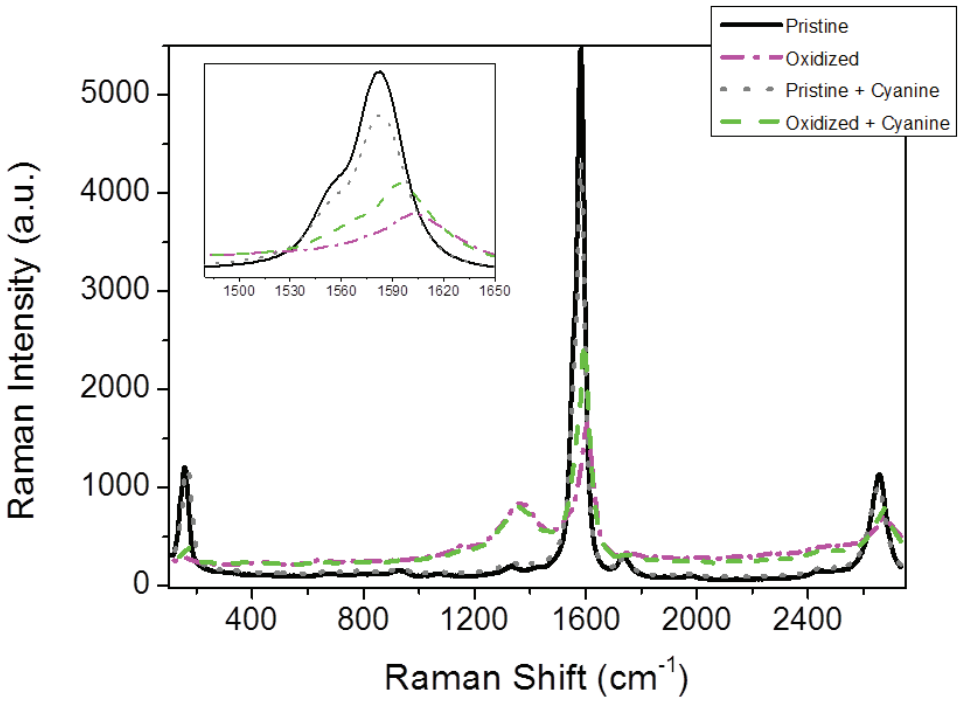

Figure 1. Single Raman spectra collected on the pristine carbon nanotube powder sample (black solid line), on the CNT sample subjected to chemical oxidation (magenta dash-dotted line) and on the CNT sample treated with cyanine dye before (grey dotted line) and after (green dashed line) the oxidation. The inset reports a magnification of the central spectral range.

The black spectrum shows some typical peaks attributed to carbon nanotubes. The more intense is the G peak, located at about 1580 cm^{-1}, which is associated with tangential vibration modes of sidewall C–C bonds, and consists of three components [9]. The D band, at about 1330 cm^{-1}, having

a much lower intensity, is ascribed to disorder-induced phonon mode of the carbon sixfold rings breathing vibration. The structured Radial Breathing Mode (RBM) is located at low Raman shifts, and has a frequency which is inversely proportional to the tube diameter. The band positioned at about 1735 cm^{-1}, called M band, is a second-order peak generally assigned to a combination mode of the G and RBM bands [9, 10], or to overtones of the out-of-plane infrared active mode at 867 cm^{1} in graphite [11, 12]. Finally, the G' band, at about 2655 cm^{-1}, is a D band overtone and represents the dominant second-order feature in SWCNT Raman spectra, with demonstrated sensitivity to doping [13, 14]. The magenta dash-dotted spectrum collected after the oxidation treatment is characterized by a considerable decrease of the G, G' and RBM band intensities, a visible increase of the D band (due to the presence of induced structural defects and sidewall disorder or amorphous carbon coating) and by the almost complete disappearance of the M band. Indeed, the ratio R between the D and G band intensities is often used to estimate the CNT structural disordering [15-17]. Moreover, all the cited bands appear up-shifted (10 to 30 cm^{-1}), as an effect of the alteration of the resonance conditions caused by specific environmental and tube-tube interactions, and by charge transfer processes due to CNT doping (such as intercalated acid molecules) [18]. As generally agreed, this sensitivity of Raman spectroscopy to surface modifications and induced defectiveness makes it an incredibly powerful technique to qualitatively assess structural changes of SWCNTs. However, things become more subtle and less obvious when trying to compare spectra obtained before and after the functionalization with dye molecules, both for the pristine and the oxidized sample. Indeed, grey dotted and black solid spectra appear quite similar, demonstrating a very slight effect of unspecific interaction of cyanine with pristine SWCNTs, mainly going in the same direction of the oxidation itself; while the CNT specific functionalization (green dashed curve) causes an opposite effect of bands increase and down-shift when compared with the just oxidized sample (magenta dash-dotted curve), as better visible in the inset reporting a magnification of the central spectral range. Furthermore, the treated samples result quite non-homogeneous, both in concentration and functionalization degree, so that Raman spectra

acquired at various points on the glass-deposited powder appear different in terms of band position and intensity (see Figure S1 in the SI). Therefore, a mapping procedure is to be preferred for a complete and accurate characterization [14]. Thus, spectra identification and interpretation, usually made through band fitting, is not at all a straightforward operation, especially when dealing with the comparison of different dyes or labeling molecules and functionalization protocols.

3.1.2 Principal Component Analysis applied to Raman maps

PCA is a multivariate statistical analysis technique widely used to reduce the dimensionality of a data set consisting of a large number of variables, while preserving most of the relevant information contained in the set. This is accomplished through a linear transformation of the variables that projects the original ones in a new Cartesian system in which new variables are sorted in descending order of variance. The complexity reduction is done by merely considering those that appear to be the main (for variance) between the new variables.

Here PCA is applied to analyse Raman spectra belonging to the maps acquired on the CNT samples with the aim of discriminating, distinguishing and comparing different degrees of CNT modification and functionalization, developing a fast, label free and reliable method to study the effects of different preparation procedures on the efficacy and homogeneity of the functionalization itself.

The results obtained on pristine, oxidized and dye treated carbon nanotubes are separately reported for the three different labeling molecules used here: R6G (Figure 2A), THA (Figure 2B) and Cy3 (Figure 2C). The structure of each dye is sketched near the corresponding graph.

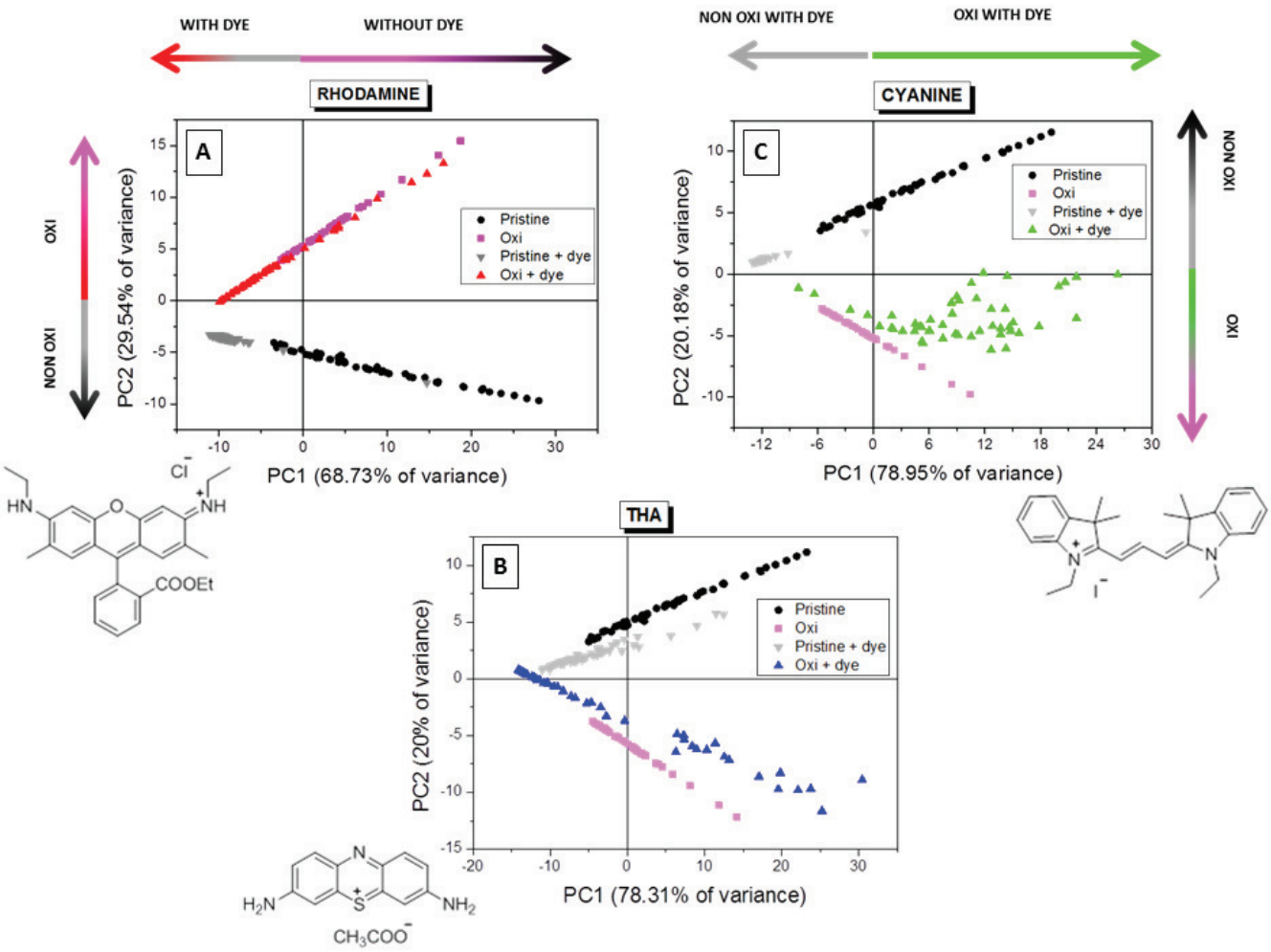

Figure 2. Results of Principal Component Analysis applied to Raman maps obtained on pristine, oxidized and dye treated pristine and oxidized carbon nanotubes for the three different used labeling molecules: **A**) R6G; **B**) THA; **C**) Cy3. The structure of each dye is sketched near the corresponding graph.

In all cases, points representing spectra belonging to different maps are clearly separated, so that, even if a certain degree of point spreading is present, an immediate distinction is possible between data obtained on non oxidized and oxidized tubes, and between CNT treated and not treated with dye molecules. In particular, focusing on Figure 2A related to rhodamine, the first principal component, PC1, well separates points corresponding to functionalized (mainly located in left half-plane) and not functionalized (mainly located in right half-plane) samples, while the second principal component, PC2, allows a net separation between oxidized (upper half-plane) and pristine

(lower half-plane) CNTs, as synthesized by the two arrows depicted parallel to the axis. An equally clear disjunction is also obtained for the other two dyes. Data reported in Figure 2B for THA similarly show, in fact, an evident distinction between pristine and oxidized samples that belong, respectively, to the upper and lower half-planes, while the PC1 component separates quite well the samples not treated with the dye (positioned on the right), and those chemically functionalized (positioned on the left), with the exception of a separated group of points discussed later in the text. The situation is peculiar for Cy3. In this case, PC2 separates, again, oxidized and non oxidized CNTs, but the functionalization gives a different localization of the map points, so that spectra of pristine treated CNTs are positioned on the left, while oxidized tubes linked to the dye appear mainly located on the right (see the arrows parallel to the axis). The shown disjunction of data points corresponding to spectra obtained on different samples demonstrates the ability of PCA applied to Raman mapping to highlight small spectral differences, even in presence of unavoidable sample inhomogeneity. Interestingly, sample inhomogeneity, together with a possible slight defocusing during the automatic mapping procedure, only causes a linear spreading of the points associated to the same map, while maps obtained in different areas of the powder sample are almost superposed, as can be verified by looking at Figure S2. This means that a single map is sufficient for a complete identification of the sample, which further demonstrates the potentiality of the approach.

Going deeper inside in data analysis, points of the same map tend to be distributed along straight lines of fixed slope, which have an opposite sign for oxidized and non oxidized CNTs, with the exception of oxidized tubes functionalized with Cy3 and THA, the first appearing substantially cloud clustered, and the second being, as already said, divided into two distinct groups differently positioned with respect to the PC1 component.

At this point, a comparison between different functionalization molecules can be also tempted by severally applying PCA to pristine treated samples, and to oxidized treated samples. The results are reported in Figures 3A and 3B, respectively.

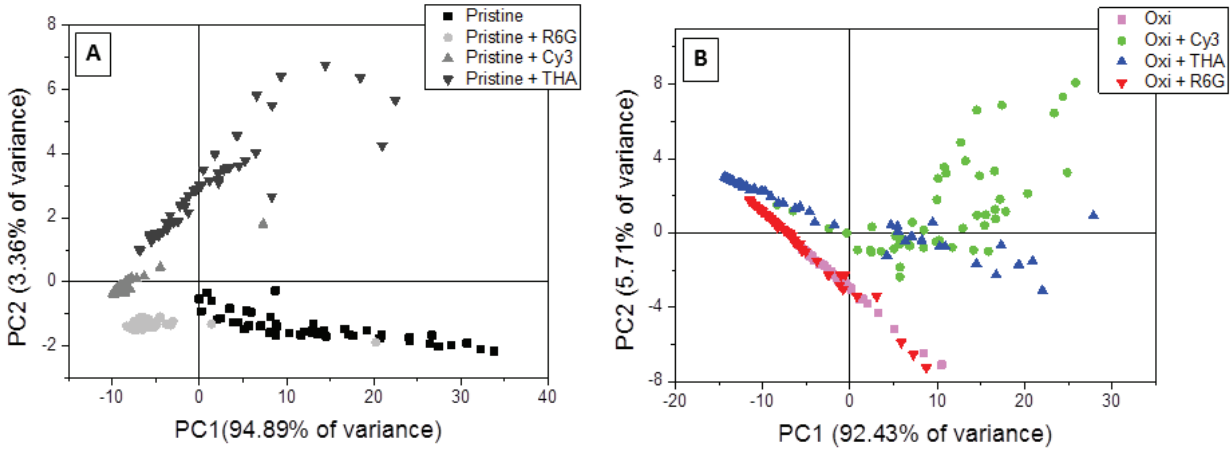

Figure 3. **A**) results of Principal Component Analysis applied to Raman maps obtained on pristine CNTs (black squares) and pristine CNTs treated with rhodamine (light grey circles), cyanine (grey up-triangles) and THA (dark-grey down-triangles). **B**) Results of Principal Component Analysis applied to Raman maps obtained on oxidized CNTs (magenta squares) and oxidized CNTs treated with cyanine (green circles), THA (blue up-triangles) and rhodamine (red down-triangles).

In the first graph, the PC1 component, which accounts for most of the data variance (almost 95%), well separates points corresponding to not functionalized tubes (black squares, positive values of the component) and those associated to the maps collected after the treatment with the dyes (negative values of the component). However, the functionalization with THA seems less effective because points (dark-grey down-triangles) appear partially spread on the right half-plane. The second component, PC2, just accounting for 3% of variance, allows to distinguish the three dyes that are vertically distributed from R6G (lower values of the component) to THA (higher values of the component).

As regards the oxidized tubes, Figure 3B shows a co-localization on the right half-plane of the cloud of points of the cyanine treated sample and points belonging to the second group associated with the functionalization with THA, indicating a similar behaviour. Differently, all the other maps are placed on the left half-plane, with PC1 components having increasing negative values from simply oxidized, to R6G and, finally, THA treated tubes.

Interestingly, the specific positioning of the spectral points only slightly depends on sample ageing. To illustrate this issue, Figure 4 presents the results of the PCA analysis when considering all the maps realized on pristine samples together, and adding points collected on similar samples but prepared at different times, i.e. pristine CNTs put in contact with cyanine molecules at the same time of the other dye molecules (Pristine + Cy3, grey up-triangles) and after 12 months (Pristine + Cy3/new, violet diamonds).

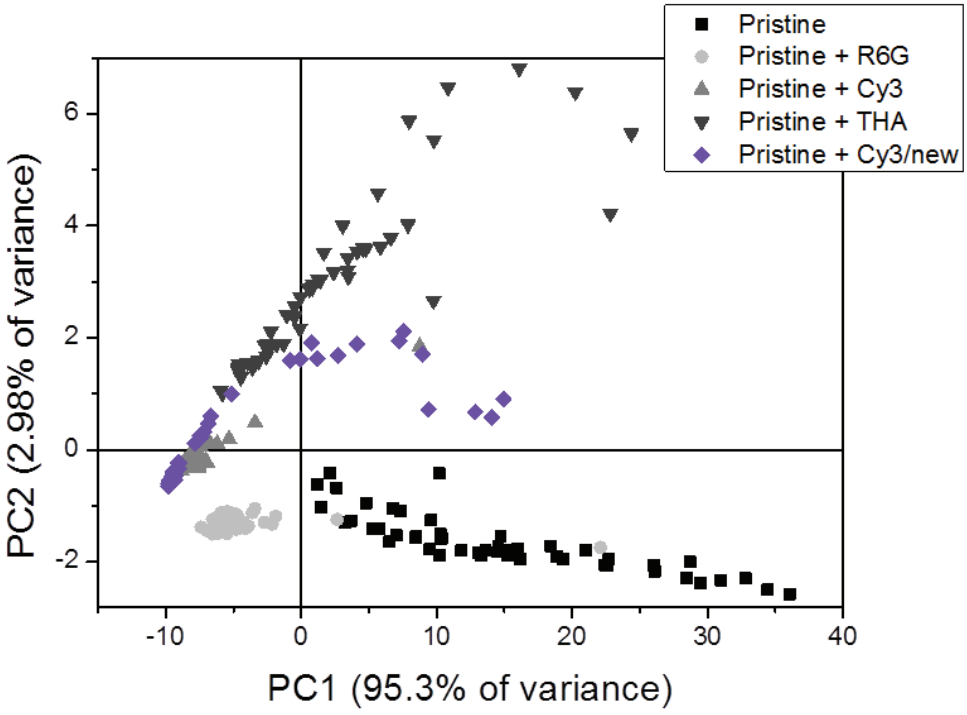

Figure 4. Results of Principal Component Analysis obtained when adding to the points associated to all the maps collected on pristine tubes, also those belonging to the maps collected on similar samples but prepared at different times, i.e. pristine CNTs put in contact with cyanine molecules at the same time of the other dye molecules (Pristine + Cy3, grey up-triangles) and after 12 months (Pristine + Cy3/new, violet diamonds).

The two differently aged samples are almost superposed in the score plot, even if the newest one is less homogeneous presenting some points located in the right half-plane of the graph. The general method is thus considerably robust, giving clustering results substantially not depending on the sample preparation.

3.2 Computational results

Molecular Interaction Fields (MIFs) were used to mimic the different interaction between the three dyes and carbon nanotubes. Briefly, the interaction energy between a small molecule or particle (called the probe) and a compound (the target, here THA, Cy3 and R6G) is calculated by positioning the probe in a 3D regular lattice of points surrounding the target. The set of interaction energy values generates a MIF typical of the compound and the probe, and thus different MIFs permit to explore various properties of the target by using different probes. Here we used two probes named Car (miming interaction with aromatic carbons) and O- (miming carboxylate atoms). We expect that MIFs derived from Car probe could mimic the interaction between the target and pristine CNTs, whereas probe O- can provide information about the interaction with carboxylic groups present on the surface of oxidized carbon nanotubes. In particular, the number of the points in the grid with energy less than a user–defined threshold gives an estimation of the propensity of the target to interact with a certain probe [19]. Figure 5 presents the results extracted by BIOCUBE-mf from GRID MIFs (see SI) for the three targets: R6G (a), Cy3 (b) and THA (c). Around the structures of the compounds, the green points correspond to those in the grid associated to an energy less than -1 kcal/mol for the probe Car, while the red points are associated to an energy less than -3.0 kcal/mol for the probe O-. The figure shows that THA appears to have an higher interaction volume for the probe O- with respect to the other two dyes.

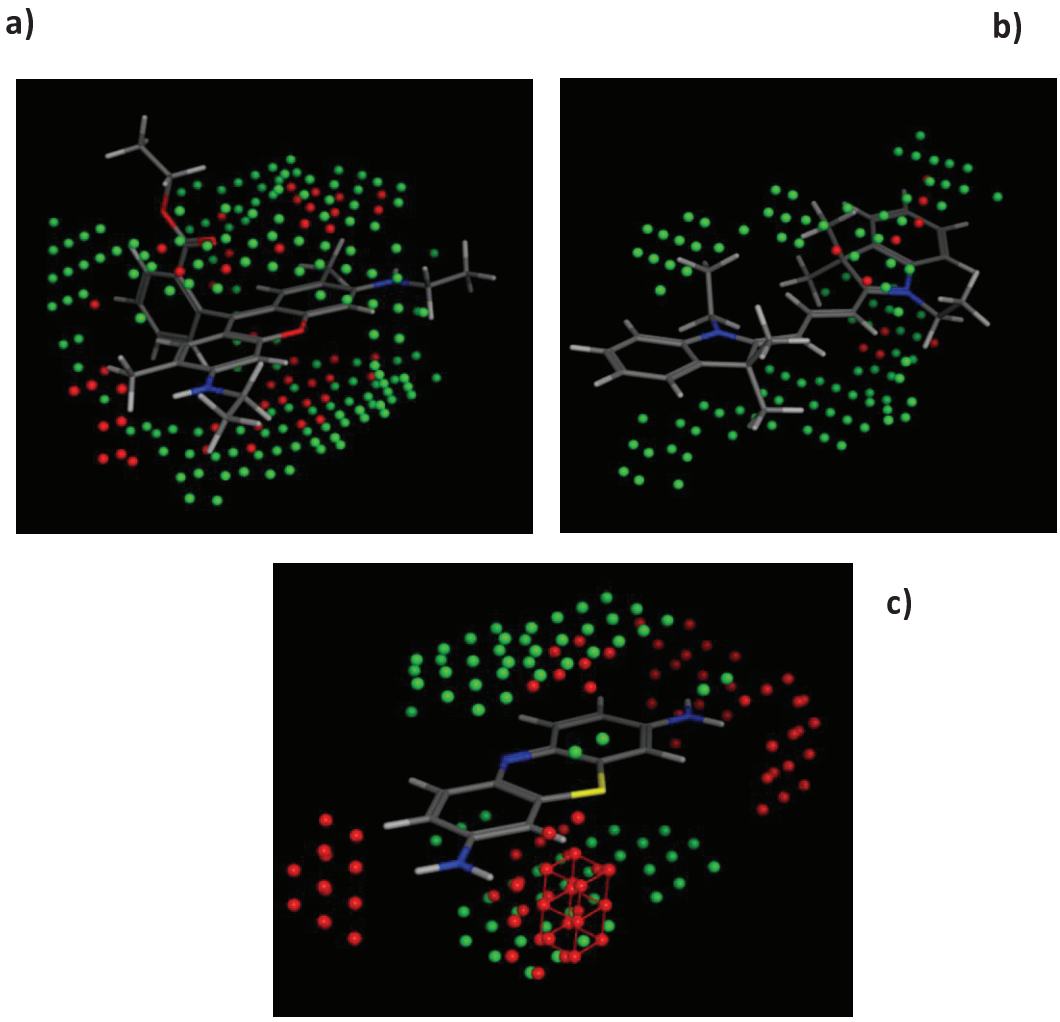

Figure 5. MIFs obtained with Car (green) and O- (red) probes for (a) R6G; (b) Cy3 and (c) THA. Car probe catch the propensity of the molecule to interact with hydrophobic regions of the nanotube, whereas O- the propensity to interact with carboxylate groups on the surface of oxidized nanotubes.

The number of points obtained by using the two probes for each compound are also reported in Table 1.

	Car (-1.0 kcal/mol)	O- (-3.0 kcal/mol)
Cyanine	98	9
Rhodamine 6G	185	11
THA	74	64

Table 1. Number of MIF points with energy less than the selected threshold calculated by BIOCUBEmf for each compound.

Molecules with higher propensity to interact with Car probe are expected to prefer interaction with apolar pristine CNTs. On the contrary, molecules with higher propensity for O- should prefer interaction with oxidized CNTs. Data in Table 1 show that R6G should interact preferably with pristine CNTs, whereas THA seems to be the one with the higher affinity with oxidized CNTs.

3.3 Thermogravimetric Analysis

Thermogravimetric analysis (TGA), in nitrogen, was performed on pristine and oxidized CNTs, as well as on the samples interacted with R6G and Cy3. The data reported in Figure 6 are in agreement with those obtained previously for THA [20], and show that the dye adsorbed on pristine CNTs does not change to a large degree the thermal stability of the sample. In fact, the small weight loss observed in the red curve with respect to the black one is due to the degradation of the dye just adsorbed by electrostatic interaction.

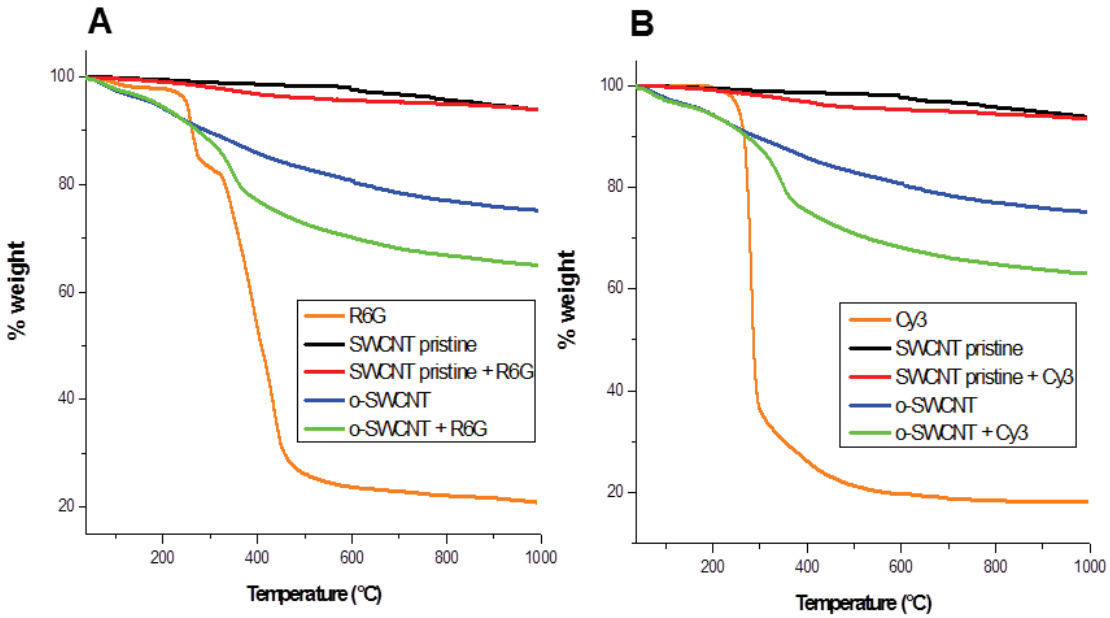

Figure 6. Thermogravimetric analysis in nitrogen flow of **A**) Rhodamine 6G, R6G, (orange), pristine CNTs (black), and oxidized CNTs (blue), and the corresponding SWCNTs with R6G (red and green); **B**) Cyanine, Cy3, (orange), pristine SWCNTs (black), and oxidized SWCNTs (blue), and the corresponding SWCNTs with Cy3 (red and green).

The weight loss is more evident for oxidized SWCNTs (o-SWCNTs), exhibiting a non-negligible weight loss in a low temperature range (100-600°C) where pristine nanotubes are extremely stable, which is due to the presence of carboxylic groups on the tube walls. Finally, the curve obtained for o-SWCNTs in the presence of the dye shows a further weight loss around 350°C, due to the organic dyes linked to the nanotubes (weight loss at 280°C for Cy3 and 260°C for R6G).

3.4 Steady-state and time-resolved fluorescence measurements

The procedure is based on the direct one step labeling of the oxidized and pristine single walled CNTs (SWCNTs) by the cationic fluorescent dyes, and the analysis of the subsequent variations in the sample fluorescence emission (see Experimental section for the full detail of the procedure). We noticed a small decrease of colour intensity when dye solutions were mixed with pristine SWCNTs, showing that pristine carbon nanotubes have a tendency to adsorb dye molecules unspecifically, as described in literature [21]. But, when the dyes are mixed with oxidized SWCNTs, the colour disappears completely in the presence of THA, and strongly decreases when R6G and Cy3 were used (see photo in Figure 7a) due to ionic pairs formation on the CNT between the dye cation (D+) and surface carboxylate groups [20]. The degree of the functionalization (i.e. how much dye is adsorbed/linked to the tubes) was studied by steady-state fluorescence measurements for every dye-CNT complex by means of a calibration graph made for each dye used. The procedure consists in removing dye-CNTs complexes after centrifugation, then filtering and titrating the solution by measuring its fluorescence emission and comparing it with calibration curve (see ESI). By difference with the initial content of the dye, the amount of fluorophore taken after interaction with different SWCNTs was evaluated and expressed as mmol of dye (Figure 7b). Moreover, to better understand the kind of the interaction of the three dyes, we calculated the difference of the concentration of the dyes in the presence of the oxidized and pristine CNTs (data not reported). These data suggest a better interaction between THA and oxidized carbon nanotubes, while R6G and partly Cy3 show a propensity to interact with nanotubes through hydrophobic and non-polar interactions.

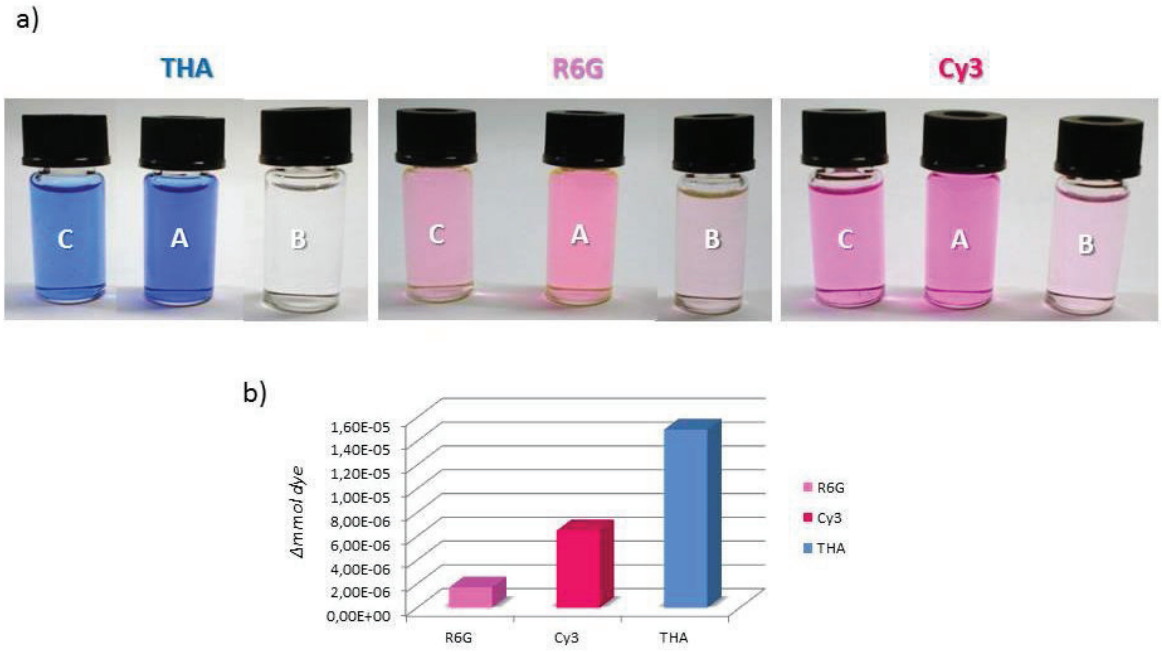

Figure 7. a) Difference in color after mixing dye stock solution (A) and oxidized CNTs, o-SWCNTs, (B), or pristine CNTS, p-SWCNTs, (C); **b**) Difference in fluorescence emission of the dyes after interaction with o-SWCNTs.

Time-resolved fluorescence measurements were also performed on the dyes in solution and on solid state, as well as on the CNT-dye complexes. Few data are available in literature, but they are in agreement with the present results [22, 23]. The fluorescence decays of the studied dyes in solution are all monoexponential with lifetimes comparable with literature data [24, 25] (see Table 2).

The analyses performed on the complexes CNT-dye on solid state shows that the decays become bi-exponential but with different behaviours caused by the different structure of the dyes used [26]. The results show that the dyes effectively interact with the different SWCNTs in two different ways depending on the type of tubes (pristine or oxidized).

In the case of R6G, its fluorescence lifetime in ethanol is 3.80 ns and 0.45 ns in the solid state, while in the presence of both pristine and functionalized CNTs the decay becomes bi-exponential with the short-lived component belonging to free R6G while the long-lived component could be attributed to the interaction between the dye and the CNTs. The differences among the three dyes are evident if we analyse the lifetime percentage between oxidized and pristine samples. In the case

of THA for example, there is quite a big difference between long-lived and short-lived lifetime percentage of pristine and oxidized CNTs showing the effectiveness of this probe to bind functionalized tubes. On the contrary, for Cy3 and R6G it's harder to find a difference in their behavior with pristine or functionalized tubes. These dyes indeed, probably due to their chemical structure, appear to interact nearly in the same way whatever the nature of the tube is.

Table 2. Fluorescence lifetime (τF) of the dyes alone (both on the solid sample and in solution in ethanol) and with the different CNTs used.

	R6G	THA	Cy3
solid	0.45 ns	0.46 ns	0.53 ns
in solution	3.8 ns (3.9 ns)[a]	0.62 ns (0.3 ns)[b]	0.15 ns
with pristine CNTs	0.31 ns [80%] 2.43 ns [20%]	0.35 ns [98%] 3.09 ns [2%]	0.34 ns [75%] 3.06 ns [25%]
with oxidized CNTs	0.31 ns [70%] 2.98 ns [30%]	0.34 ns [86%] 2.55 ns [14%]	0.30 ns [65%] 2.74 ns [35%]

[a)] in methanol, [25]; [b)] in water [24]. Lifetime percentages are reported in square brackets.

4. Discussion

The substantial agreement between the results obtained with different techniques and presented in section 2 is remarkable, and allows to better interpret those of PCA applied to Raman maps. Notably, one can even draft a sort of classification of dye molecules with respect of functionalization efficiency: as regards oxidized samples, THA molecules better link to CNTs than R6G, while Cy3 seems to be the less effective; differently, R6G and Cy3 show a propensity to interact with nanotubes through hydrophobic and non-polar interactions. This rough classification appears quite clear when analysing the numbers reported in Table 1 obtained with computational methods, but it is also confirmed by the fluorescent data, summarized in Figure 7 and table 2. TGA measurements confirm these assignments, showing a distinct behaviour for pristine dye-treated and oxidized dye-treated CNTs, due to the different content of superficial carboxylate groups. Given this general understanding, one can quite easily read and explain the point positioning in the score plots obtained when applied PCA to the Raman maps collected on the various samples. Starting from the data reported in figure 3A for pristine tubes, one can infer that the PC2 component

accounts for the dye propensity to unspecifically interact with the CNTs surface. In this picture, the vertical distribution from R6G (lower values of the component) to THA (higher values of the component) reflects a decreasing efficiency of interaction, also confirmed by the fact that some of the points obtained on the THA treated sample encroach the right half-plane where not functionalized tubes are positioned. Conversely, as far as the arrangement of the points is concerned, the functionalization of oxidized CNTs with THA produces spectra associated with larger negative values of the PC1 component, as shown in figure 3B, thus locating farther away with respect to simply oxidized tubes and extending on the left side of the graph. The PC1 component, having increasing negative values from simply oxidized, to R6G, and, finally, THA treated tubes, can thus be related to the functionalization efficiency when considering oxidized samples. The spreading of the points corresponding to the Cy3 interacted sample, mainly located in the right half-plane, confirms, instead, the computational results that indicate a slightly smaller interaction volume. Nevertheless, one can also notice a distribution of the maps along the PC2 component increasing from points belonging to the maps realized on simply oxidized, to R6G and THA treated tubes. This component also could be partly associated to the functionalization efficiency, explaining the inverted classification between R6G and Cy3 obtained with fluorescence measurements, correlated to the high PC2 values of some points of the non-homogeneous cloud of cyanine functionalized CNTs.

It is interesting to note that in figure 3B THA presents two clusters of points, differently located in the score plot. This finding seems to mean that THA molecules are able to link to oxidized CNTs with two distinguishable mechanisms associated to different efficiencies, one similar to that typical of the interaction of cyanine molecules with the CNTs surface, and one more stable and effective, giving raise to spectral points with lower values of PC1 component. This conclusion, which is only inferable when applying multivariate analysis to Raman spectra and not deducible by the other experimental techniques, appear supported by the analysis of the MIFs of cyanine and THA. These compounds share an aromatic cyclic portion of the structure that interacts with the Car, as shown by

green points in figure 5, suggesting a first common weak interaction mechanism; furthermore, THA can strongly interact with the O- probe suggesting the presence of a second more efficient mechanism of interaction with CNTs.

The proposed method, applied to study the functionalization process and compare different labeling molecules, appears really robust and trustworthy, especially considering that the results obtained with differently aged samples are impressively coherent: by looking at figure 4 one can notice that the maps realized on pristine tubes treated with Cy3 at different times have the same position with respect to PC2, which is supposed to be related to the effectiveness of the functionalization, i.e. to the propensity of the dye to interact with the CNTs. Interestingly, the data representation also accounts for smaller differences always present in the multi-step preparation procedure, given that the map associated to the newest sample contains spread points located in the right half-plane, indicating a greater non homogeneity in the functionalization efficiency.

5. Conclusion

The presented results clearly demonstrate the ability of Principal Component Analysis applied to Raman mapping to simply distinguish different CNTs samples on the basis of the degree of oxidation, efficiency of functionalization, molecule labeling and treatment homogeneity. The procedure can be applied with confidence to the study and comparison of final products, and represents a reliable method for the fast screening of functional nanostructures based on carbon nanotubes in several fields, such as bio-imaging, drug delivery, toxicology, chemical mapping. In particular, this study allowed to compile a real grading of the propensity of the studied dye molecules to interact with CNTs: rhodamine 6G and cyanine preferably link to pristine tubes, via hydrophobic and non-polar interactions, whereas THA prefers oxidized samples, rich of carboxylic groups. Moreover, the functionalization with cyanine appears less homogeneous, and the graphical outcome of the PCA analysis does not critically depend on the sample ageing. These results may be

important for a detailed characterization of the properties of the nano-hybrid materials and for an accurate proof of their actual effectiveness, especially for biomedical purposes.

Acknowledgments

SV acknowledges financial support by NANOMED project (PRIN 2010-2011, 2010FPTBSH_003) from Ministero dell'Istruzione, dell'Università e della Ricerca.

References

[1] A. Albini, V. Mussi, A. Parodi, A. Ventura, E. Principi, S. Tegami et al., *Nanomedicine: Nanotechnology, Biology, and Medicine*, 2010, **6**, 277-288.

[2] E. Gaufrs, N.Y. Wa Tang, F. Lapointe, J. Cabana, M.A. Nadon, N. Cottenye, F. Raymond, T. Szkopek and R. Martel, *Nature Photonics*, 2014, **8**, 72-78.

[3] P. Knief, C. Clarke, E. Herzog, M. Davoren, F. M. Lyng, A. D. Meade, and H. J. Byrne, *Analyst*, 2009, **134**, 1182-1191.

[4] R. Y. Sato-Berrú, E.V. Basiuk (Golovataya-Dzhymbeeva) and J. M. Saniger, *J. Raman Spectrosc.*, 2006, **37**, 1302-1306.

[5] Spartan '10; Wavefunction, Inc.: Irvine, CA, 2010.

[6] J.M. Dewar, E.G. Zoebisch, E.F. Eamonn, J.J.P. Stewart, *J Am. Chem. Soc.*, 1985, **107** (13), 3902-3909.

[7] G. Caron, A. Nurisso, G. Ermondi, *Chem. Med. Chem.*, 2009, **4**, 29-36.

[8] GRID v. 22c Molecular Discovery Ltd. Pinner, Middlesex, UK, 2009, http://www.moldiscovery.com.

[9] S. S. Islam, K. A. Shah, H. S. Mavi, A. K. Shaukla, S. Rath and Harsh, *Bull. Mater. Sci.*, 2007, **30**, 295-299.

[10] S.D.S. Brown, P. Corio, A. Marucci, M.A. Pimenta, M.S. Dresselhaus, G. Dresselhaus, *Phys Rev B*, 2000, **61**, 7734-7742.

[11] V.W. Brar, G.G. Samsonidze M.S. Dresselhaus, G.Dresselhaus, R. Saito, A.K. Swan, et al. *Phys Rev B*, 2001, **66**, 155418-155427.

[12] Y. Kawashima, G. Katagiri, *Phys Rev B*, 1999, **59**, 62-64.

[13] R. Rao, J. Reppert, R. Podila, X. Zhang, A. M. Rao, S. Talapatra, B. Maruyama, *CARBON,* 2011, **49**, 1318-1325.

[14] V. Mussi, C. Biale, S. Visentin, N. Barbero, M. Rocchia, U. Valbusa, *CARBON,* 2010, **48**, 3391-3398.

[15] S. Osswald, M. Havel, Y. Gogotsi, *J. Raman Spec.*, 2007, **38**, 728-736.

[16] F. Tuinstra, J.L. Koenig, *J Chem. Phys.*, 1970, **53**, 1126-1130.

[17] S. Bandow, A.M. Rao, G.U. Sumanasekera, P.C. Eklund, F. Kokai, K. Takahashi, et al., *Appl Phys A*, 2000, **71**, 561-564.

[18] M. S. Dresselhaus, G. Dresselhaus, R. Saito, A. Jorio, *Physics Reports*, 2005, **409**, 47-99.

[19] G. Cruciani, P. Crivori, P.-A. Carrupt, B. Testa, *J. Mol. Struct.* (Theochem), 2000, **503**, 17-30.

[20] S. Visentin, N. Barbero, S. Musso, V. Mussi, C. Biale, R. Ploeger et al, *Chem. Commun*., 2010, **46**, 1443-1445.

[21] Q. Li, J. Zhang, H. Yan, M. He, Z. Liu, *CARBON*, 2004, **42**, 287-291.

[22] S. Tapasi and P. Amitava *J. Phys. Chem. C*, 2008, **112**, 3216-3222.

[23] V. Martínez Martínez, F. López Arbeloa, J. Bañuelos Prieto, and I. López Arbeloa, *J. Phys. Chem. B*, 2005, **109**, 7443-7450.

[24] P. Natarajan, C. Raja, *European Polymer Journal*, 2005, **41**, 2496-2504.

[25] W. Holzer, H. Gratz, T. Schmitt, A. Penzkofer, A. Costela, I. García-Moreno, R. Sastre, F.J. Duarte, *Chemical Physics*, 2000, **256**, 125-136.

[26] P. Kubát, K. Lang, P. Janda, O. Frank, I. Matulková, J. Sýkora, S. Civiš, M. Hof and L. Kavan, *J. Nanosci. Nanotechnol.*, 2009, **9**, 5795-5802.

Multivariate Analysis is successfully applied to Raman mapping of carbon nanotubes at different degree of oxidation and functionalization with dye labeling molecules. The proposed methodology, that allows a fast and reliable classification of samples, could represent a powerful and routine test for the rational design of functional nanostructures.

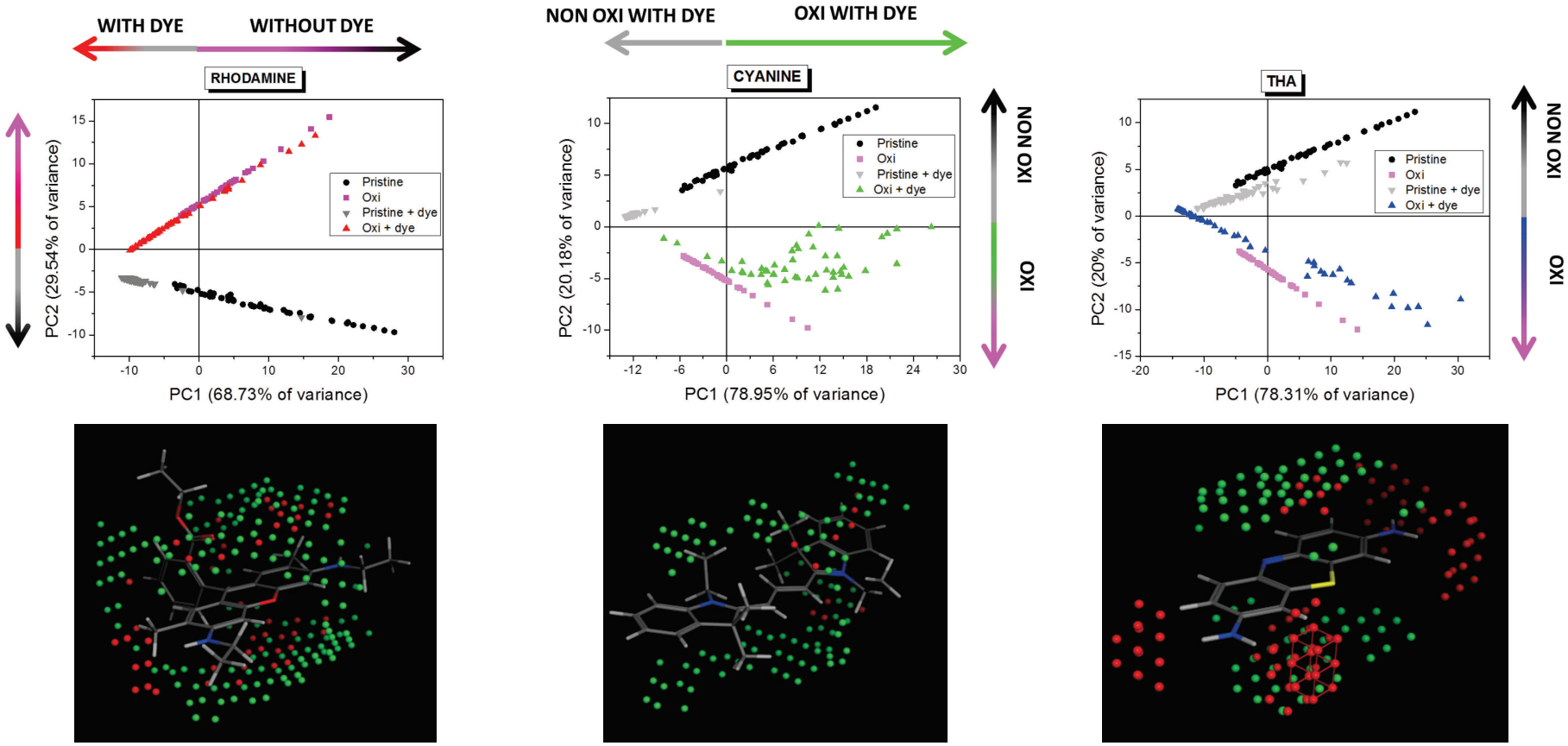

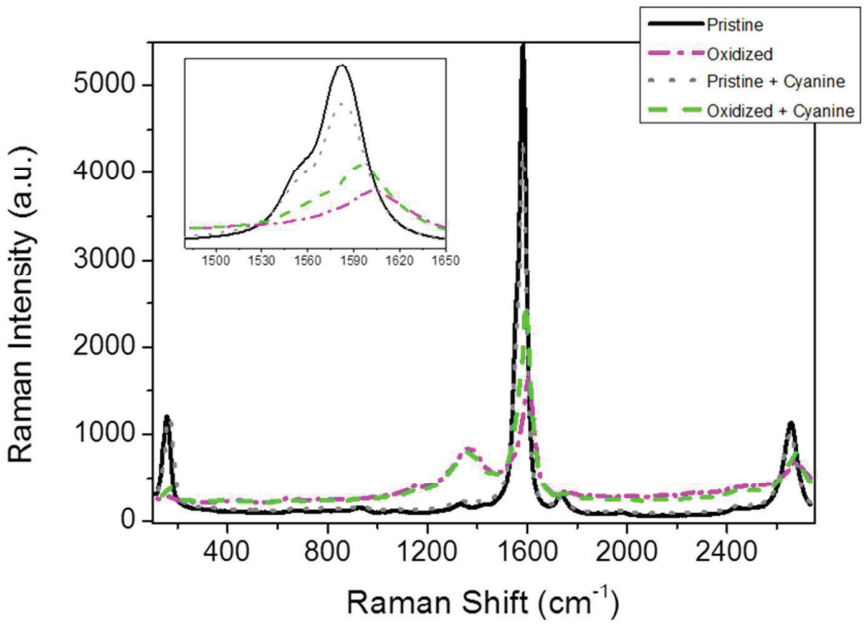

Single Raman spectra collected on the pristine carbon nanotube powder sample (black solid line), on the CNT sample subjected to chemical oxidation (magenta dash-dotted line) and on the CNT sample treated with cyanine dye before (grey dotted line) and after (green dashed line) the oxidation. The inset reports a magnification of the central spectral range.
254x190mm (96 x 96 DPI)

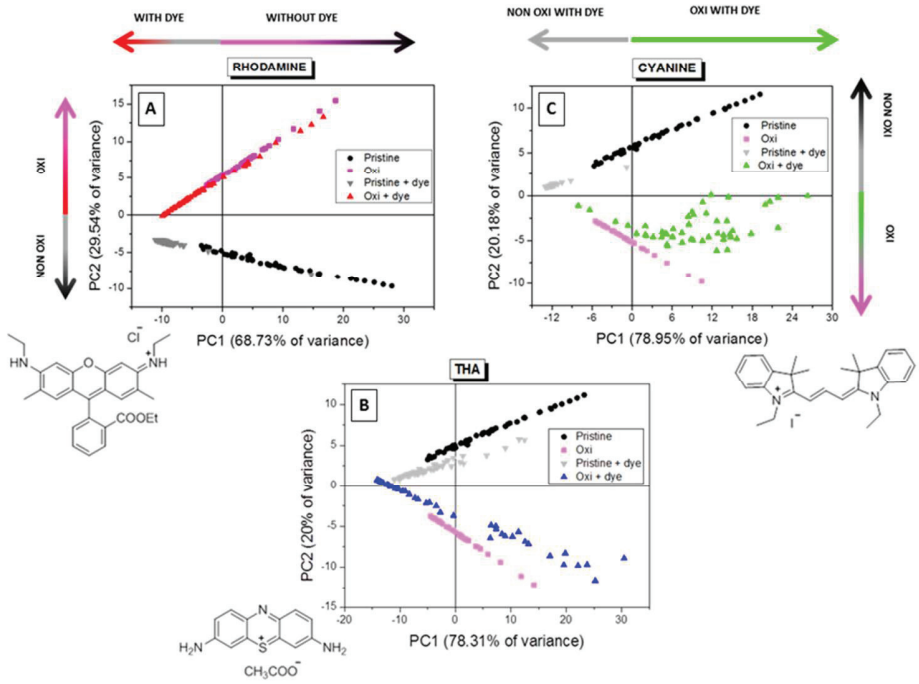

Results of Principal Component Analysis applied to Raman maps obtained on pristine, oxidized and dye treated pristine and oxidized carbon nanotubes for the three different used labeling molecules: A) R6G; B) THA; C) Cy3. The structure of each dye is sketched near the corresponding graph.
254x190mm (96 x 96 DPI)

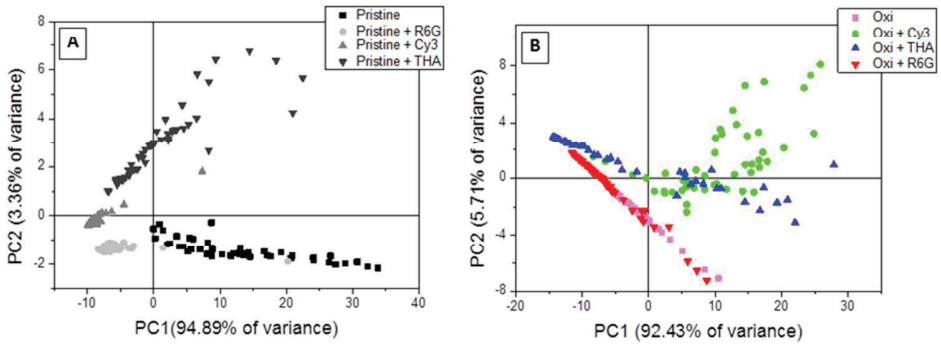

A) results of Principal Component Analysis applied to Raman maps obtained on pristine CNTs (black squares) and pristine CNTs treated with rhodamine (light grey circles), cyanine (grey up-triangles) and THA (dark-grey down-triangles). B) Results of Principal Component Analysis applied to Raman maps obtained on oxidized CNTs (magenta squares) and oxidized CNTs treated with cyanine (green circles), THA (blue up-triangles) and rhodamine (red down-triangles).
254x190mm (96 x 96 DPI)

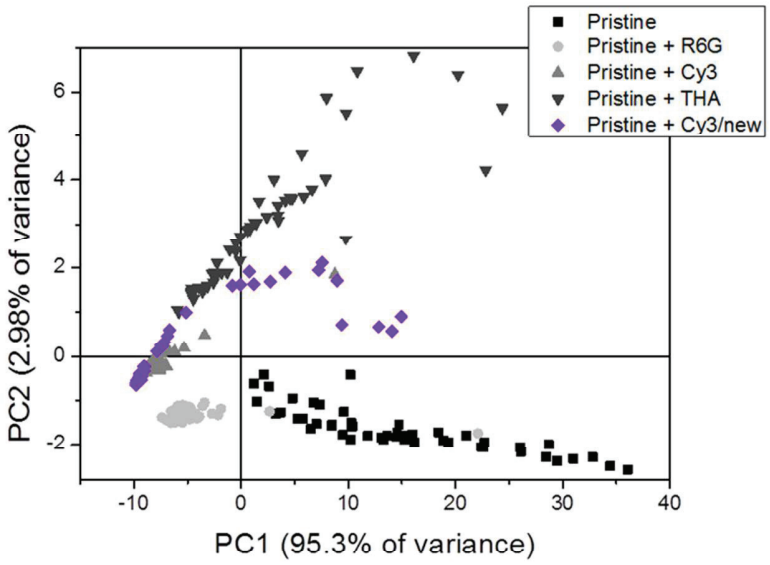

Results of Principal Component Analysis obtained when adding to the points associated to all the maps collected on pristine tubes, also those belonging to the maps collected on similar samples but prepared at different times, i.e. pristine CNTs put in contact with cyanine molecules at the same time of the other dye molecules (Pristine + Cy3, grey up-triangles) and after 12 months (Pristine + Cy3/new, violet diamonds).
254x190mm (96 x 96 DPI)

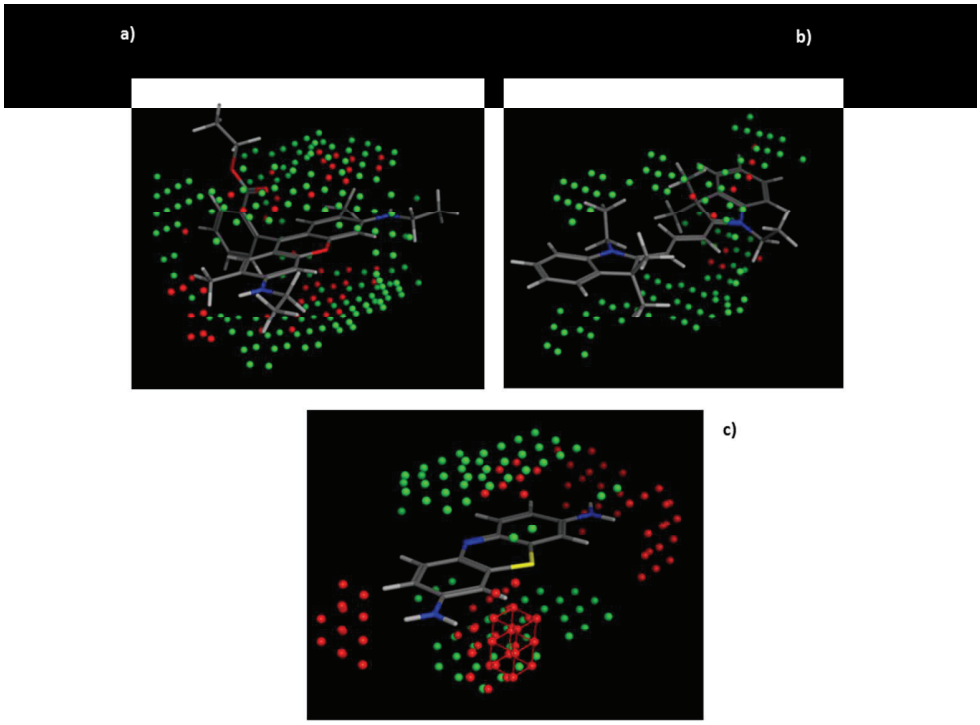

MIFs obtained with Car (green) and O- (red) probes for (a) R6G; (b) Cy3 and (c) THA. Car probe catch the propensity of the molecule to interact with hydrophobic regions of the nanotube, whereas O- the propensity to interact with carboxylate groups on the surface of oxidized nanotubes.
254x190mm (96 x 96 DPI)

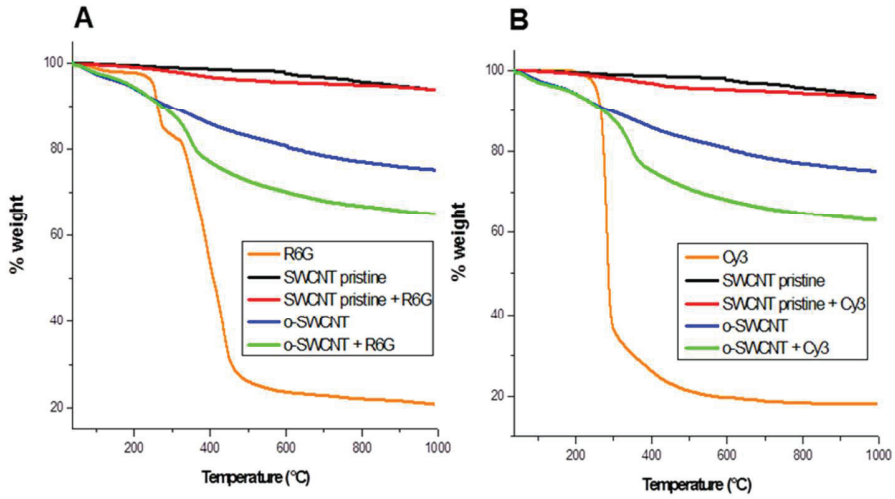

Thermogravimetric analysis in nitrogen flow of A) Rhodamine 6G, R6G, (orange), pristine CNTs (black), and oxidized CNTs (blue), and the corresponding SWCNTs with R6G (red and green); B) Cyanine, Cy3, (orange), pristine SWCNTs (black), and oxidized SWCNTs (blue), and the corresponding SWCNTs with Cy3 (red and green).
254x190mm (96 x 96 DPI)

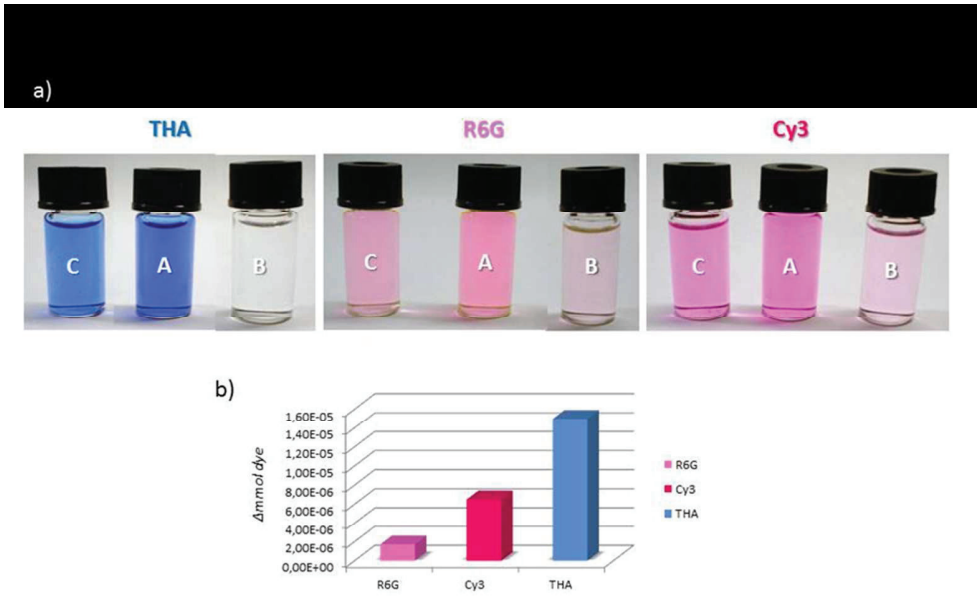

a) Difference in color after mixing dye stock solution (A) and oxidized CNTs, o-SWCNTs, (B), or pristine CNTS, p-SWCNTs, (C); b) Difference in fluorescence emission of the dyes after interaction with o-SWCNTs.
254x190mm (96 x 96 DPI)

Supplementary Information

Multivariate Analysis Applied to Raman Mapping of dye-functionalized Carbon nanotubes: a novel approach to support the rational design of functional nanostructures

*Sonja Visentin, Nadia Barbero, Francesca Romana Bertani, Mariangela Cestelli Guidi, Giuseppe Ermondi, Guido Viscardi and Valentina Mussi**

Raman measurements

Subtle differences can be identified in the Raman spectra acquired at different positions of the same sample. Figure S1 shows two spectra obtained at different points on the powder sample of oxidized CNTs treated with cyanine.

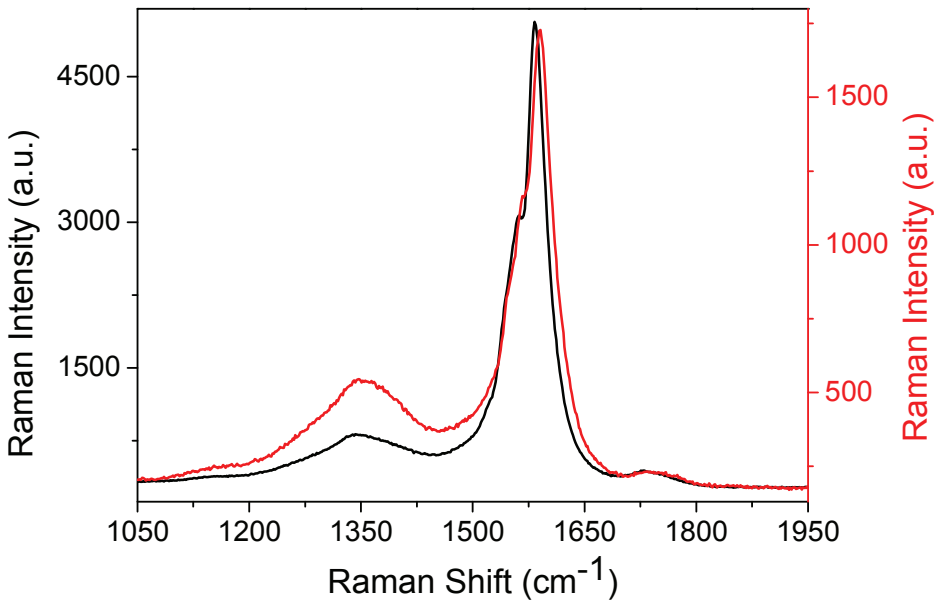

Figure S1

Figure S2 presents the results of Principal Component Analysis obtained when considering maps collected on pristine CNTs (black circles), on pristine CNTs treated with rhodamine (grey down-triangles), on oxidized CNTs (magenta squares) and in two different areas of the powder sample of

oxidized CNTs treated with rhodamine (red up-triangles and orange diamonds). The last two maps are almost superposed.

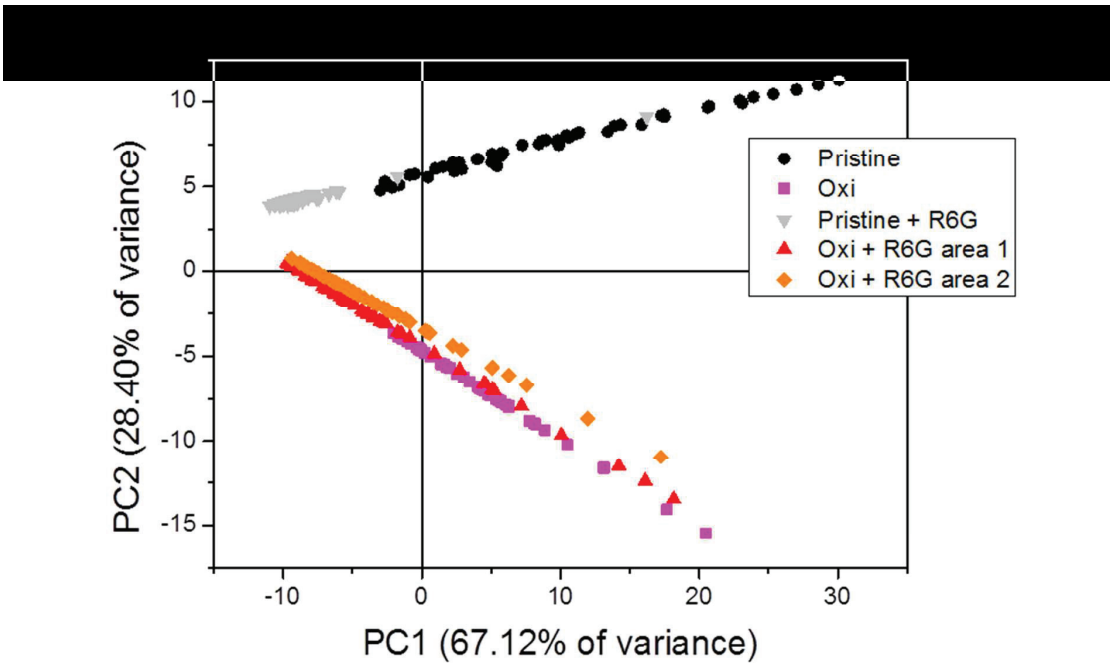

Figure S2.

Figure S3 shows the comparison between the results obtained with Principal Component Analysis applied to Raman maps collected on differently treated CNTs when using the Covariance matrix (left side) and the Correlation matrix (right side).

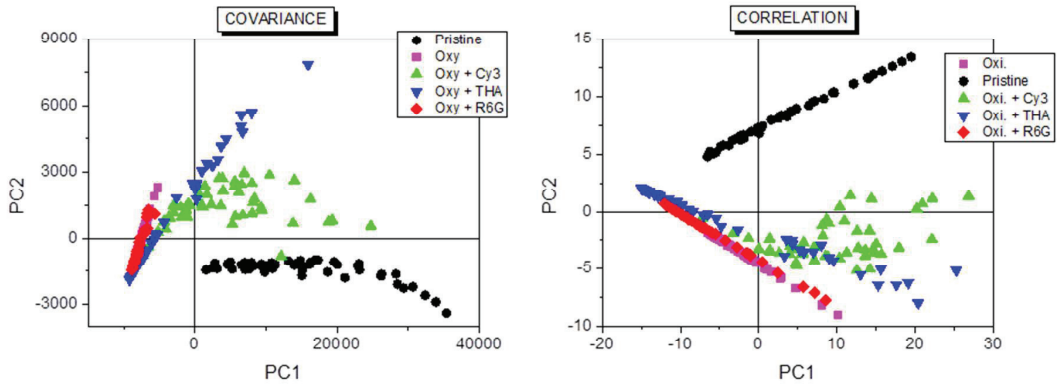

Figure S3

Table S1 contains the complete list of the wavelengths used for the Principal Components Analysis. The wavelengths are chosen in the spectral ranges corresponding to the RBM, D, G, M and G' bands, as indicated in the Table.

Table S1

Spectral Band	Wavelength (nm)	Spectral Band	Wavelength (nm)	Spectral Band	Wavelength (nm)	Spectral Band	Wavelength (nm)	Spectral Band	Wavelength (nm)
R B M	109.12454	D	1239.74	G	1470.1949	M	1700.123	G ‘	2403.2261
	120.7914		1249.9067		1480.0563		1709.6799		2413.293
	130.5045		1260.0598		1489.9047		1720.8156		2423.344
	140.2053		1270.1992		1499.74		1730.3458		2433.3813
	149.8940		1280.3251		1509.5623		1739.8636		2441.9712
	159.5746		1290.4374		1519.3716		1750.9512		2443.4011
	169.2431		1300.5361		1530.8003		1760.4424		2453.4075
	180.8309		1310.6232		1540.5819		1771.4996		2463.3962
	190.4752		1320.6949		1550.3506		1780.9628		2473.3716
	200.1096		1330.7551		1560.1064		1790.4137		2483.3313
	209.7320		1339.1261		1561.7311		1801.4232		2493.2739
	219.3464		1350.8334		1564.9794				2503.2029
	230.8677		1360.8514		1568.2264				2513.1167
	240.4561		1370.858		1571.4705				2523.0151
			1380.8512		1574.7151				2534.3074
			1390.8312		1577.9585				2544.1736
			1400.7979		1581.1989				2554.0247
			1410.7513		1584.438				2563.8589
			1420.6915		1587.6777				2573.6797
			1430.6185		1589.2953				2582.0845
			1440.5323		1590.9144				2590.4775
			1450.433		1600.6154				2591.8767
			1460.3206		1610.3055				2603.0483
					1621.5925				2612.8088
					1631.2537				2623.9436
					1640.9038				2633.6709
					1650.5397				2643.3835
					1660.1627				2653.0813
					1671.3738				2662.7642
					1680.97				2672.4324
					1690.5519				2682.0842
									2691.7229
									2702.7192
									2713.6973
									2723.2871
									2732.8608

Oxidation procedure of pristine SWCNTs

Pristine SWCNTs, purchased from Sigma Aldrich have been oxidized by acid treatment as following: the SWCNT containing powder was ultrasonicated at 40°C in a highly acidic 3:1 mixture of H_2SO_4 and HNO_3 for 3 hours. The as collected filtered powder (oxidized SWCNTs) was then characterized.

Spectrochemical titration

In Figure S4, panel a), fluorescence spectra of THA at different concentrations are shown as an example of spectrochemical titration. Panel b) presents the calibration curves for THA, R6G and Cy3 (three to five points from 9.7 x 10^{-8} to 2.4 x 10^{-7}; mother solution 9.7 x 10^{-5}) done by using the fluorimetric method described in the experimental section of the paper ($R^2 = 0.999$).

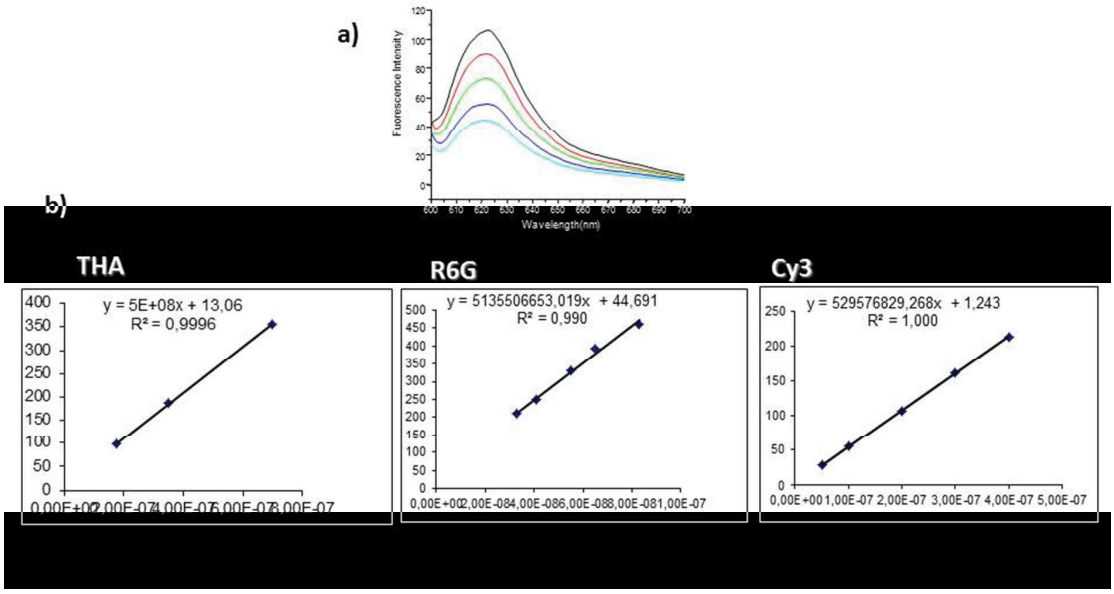

Figure S4

Figure S5 shows examples of fluorescent spectra of dyes reacted with pristine SWCNTs (p-SW) and oxidized SWCNTs (f-SWCNTs). For non oxidized nanotubes the resulting dye solution was diluted 400 times

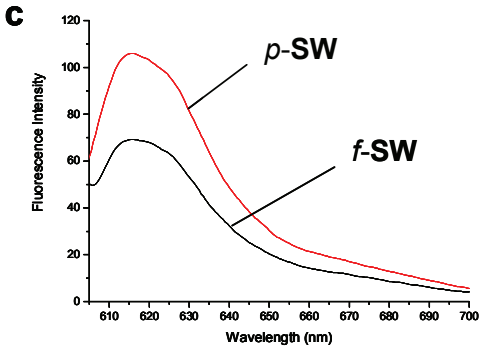

Figure S5